

RSC Advances

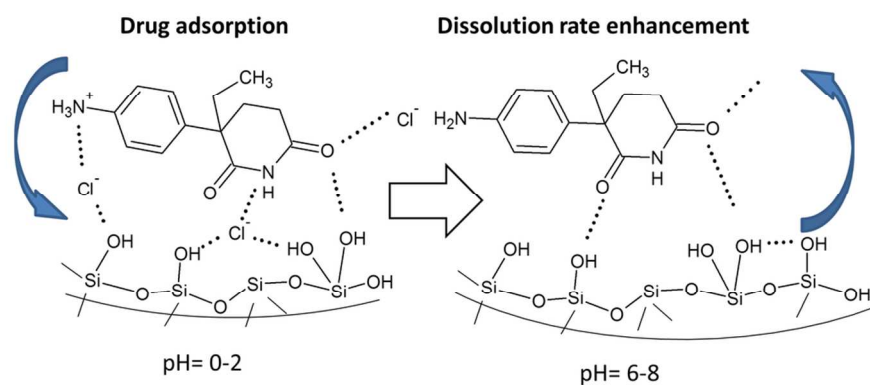


This is an *Accepted Manuscript*, which has been through the Royal Society of Chemistry peer review process and has been accepted for publication.

Accepted Manuscripts are published online shortly after acceptance, before technical editing, formatting and proof reading. Using this free service, authors can make their results available to the community, in citable form, before we publish the edited article. This *Accepted Manuscript* will be replaced by the edited, formatted and paginated article as soon as this is available.

You can find more information about *Accepted Manuscripts* in the [Information for Authors](#).

Please note that technical editing may introduce minor changes to the text and/or graphics, which may alter content. The journal's standard [Terms & Conditions](#) and the [Ethical guidelines](#) still apply. In no event shall the Royal Society of Chemistry be held responsible for any errors or omissions in this *Accepted Manuscript* or any consequences arising from the use of any information it contains.



Chlorine ions can mediate the adsorption and enhance the dissolution release of aminoglutethimide from pristine and functionalized MCM-41 mesoporous silica.
99x39mm (300 x 300 DPI)

Tailoring the dissolution rate enhancement of aminoglutethimide by functionalization of MCM-41 silica: a hydrogen bonding propensity approach

Raul – Augustin Mitran^{1,2}, Silviu Năstase¹, Cristian Matei¹, Daniela Berger^{1*}

¹ University "Politehnica" of Bucharest, Faculty of Applied Chemistry and Material Science, 1-7 Polizu street, Bucharest, 011061, Romania

² SARA Pharm Solutions, 266–268 Calea Rahovei, Bucharest, 050912, Romania

Abstract

The adsorption and *in vitro* release properties of the poorly soluble cytostatic agent DL-aminoglutethimide (AGT) on pristine MCM-41, 3-aminopropyl and a novel N-propyl-2-sulfanylacetamide functionalized MCM-41 materials were studied. The mesostructured supports and hybrid samples were characterized by small- and wide-angle X-ray diffraction, FT-IR spectroscopy, thermogravimetric and calorimetric analyses, SEM-EDX and N₂ adsorption-desorption isotherms. The drug uptake was found to be strongly influenced by its ionization state and solution pH. Drug release experiments show a spectacular increase in dissolution rate of therapeutic agent for all hybrid samples, indicating that aminoglutethimide encapsulation into the mesopores of MCM-41-type supports is a viable strategy for dissolution rate enhancement. Using a knowledge-based logit hydrogen bonding propensity model to assess the relative strengths of drug-support supramolecular interactions, we have proposed that a Si-OH \cdots Cl⁻ AGT⁺ mechanism is responsible for the increased drug adsorption in acid media and release rate enhancement at physiological pH.

Keywords: hydrogen bonding propensity, mesoporous silica, dissolution rate enhancement, aminoglutethimide, functionalized MCM-41

Introduction

Mesoporous silica nanoparticles are promising carriers for obtaining drug delivery systems with applications such as targeted drug delivery¹, controlled release² and solubility enhancement³ due to their good adsorbent properties, non-toxicity and biocompatibility^{4,5}. Moreover, the mesoporous silica properties can be easily tailored through synthesis by the incorporation of different atoms into the silica framework^{6, 7}, grafting of organic groups into mesochannels⁸⁻¹⁰, controlling the pores size¹¹ and their arrangement^{12,13}, as well as nanoparticles morphology¹⁴⁻¹⁷.

DL-Aminoglutethimide, (\pm)-3-(4-aminophenyl)-3-ethyl-piperidine-2,6-dione (AGT), an aromatase inhibitor¹⁸ used in the treatment of breast cancer¹⁹ and Cushing's syndrome²⁰ was chosen as a model molecule in this work. AGT has a low water solubility and good permeability, being considered a

* Corresponding author: Daniela Berger Tel. +40 214023986 e-mail: danaberger01@yahoo.com

class II drug according to the Biopharmaceutics Classification System, with solubility as the limiting factor in adsorption and bioavailability. Therefore an increase in dissolution rate or solubility can improve the therapeutic effect. In the previous reports mesoporous silica encapsulation has been shown as a good strategy to increase the dissolution rate of poorly soluble drugs like naproxen²¹, ibuprofen²² and carbamazepine²³. Moreover, the model drug is structurally related to phenobarbital and phenytoin and it contains the imide functional group, a common drug synthon which can participate in various supramolecular interactions.

To date, the encapsulation of aminoglutethimide in mesoporous silica and its subsequent *in vitro* release was not studied. The present work was aimed at exploring the possibilities of AGT dissolution rate enhancement through encapsulation in pristine and functionalized MCM-41-type silica supports. A novel functionalized MCM-41 material containing N-propyl-2-sulfanylacetamide groups grafted on silica pore walls was synthesized and employed in comparison with 3-aminopropyl functionalized MCM-41 to assess the influence of different organic groups on AGT encapsulation and release in simulated body fluid (saline phosphate buffer solution, pH=7.4). The N-propyl-2-sulfanylacetamide functionalization was chosen due to the possibility of hydrogen bonding formation with the amide – based synthons, found in many drugs.

As demonstrated recently, in the case of acetylsalicylic acid and ibuprofen²⁴, the drug-silica interactions are dominated by dispersion and hydrogen bonding effects. In the present work, we have employed a logit hydrogen bonding propensity (LHP) model^{25,26} to qualitatively assess the strength of hydrogen bonding between water, silica supports and their organic moieties bound on the pore walls and both neutral and ionized AGT molecules. Based on the LHP model results, the AGT incorporation and delivery profile could be explained. To the best of our knowledge, the LHP model has not been previously employed to describe the supramolecular interactions in mesoporous silica-type materials.

Experimental

Materials

Mesoporous MCM-41 silica (Aldrich), (3-aminopropyl)triethoxysilane (APTES, Sigma–Aldrich), thioglycolic acid (Sigma–Aldrich), N,N'-diisopropylcarbodiimide (DIC, Aldrich), N-hydroxysuccinimide (HOSu, Fluka), DL-aminoglutethimide (Aldrich) and solvents (Sigma–Aldrich) were used as received.

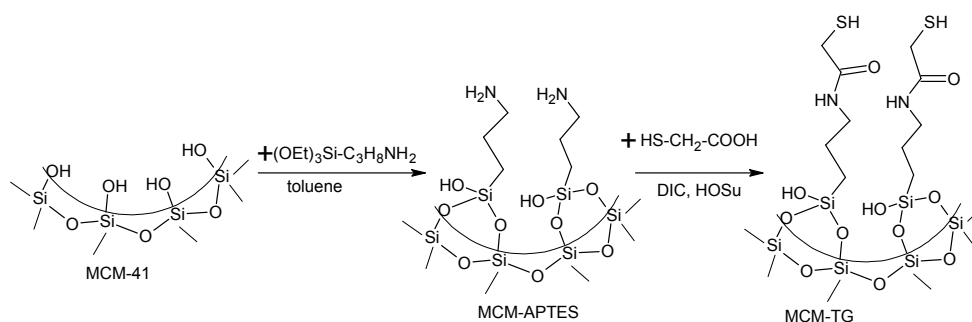
Synthesis of 3-aminopropyl functionalized MCM-41 material (MCM-APTES)

The pore surface modification of MCM-41 material with 3-aminopropyl groups was carried out by silylation method²⁷. Briefly, 0.7 g MCM-41 was dried at 110 °C for 1 h under vacuum and dispersed in

35 mL toluene and then 0.7 mL (3 mmol) APTES was added. The reaction mixture was heated at reflux for 4 h. The functionalized solid, labelled MCM-APTES, was recovered by centrifugation, washed with toluene, absolute ethanol and 0.1 M HCl aqueous solution and then dried in air at room temperature.

Synthesis of N-propyl-2-sulfanylacetamide functionalized MCM-41 material (MCM-TG)

A novel N-propyl-2-sulfanylacetamide functionalized MCM-41 material (MCM-TG) was prepared by suspending 0.18 g MCM-APTES in 10 mL acetonitrile under magnetic stirring, followed by the addition of a solution containing 75 μ L N,N'-diisopropylcarbodiimide (1 mmol), 0.115 g N-hydroxysuccinimide (1 mmol), 70 μ L thioglycolic acid (1 mmol), 335 μ L hexadecyldimethylamine (1 mmol) in 2 mL acetonitrile at room temperature. The reaction mixture was stirred for 18 h at 25 $^{\circ}$ C (Scheme 1). The solid was recovered by centrifugation, washed twice with acetonitrile and ethanol and air-dried.



Scheme 1. MCM-41 pore wall functionalization with APTES and subsequent condensation reaction with thioglycolic acid

Drug loading and *in vitro* release studies

Drug loading onto the mesoporous matrices was carried out by solution impregnation. Usually, 0.1 g support was out-gassed for 1 h at 110 $^{\circ}$ C under vacuum. A solution containing 0.1 g drug was added and kept under magnetic stirring for 24 h. Acetonitrile, ethanol or acidic (HCl) aqueous solution were used. In the case of acidic solutions, an excess of HCl was employed in order to ensure sufficiently acid pH for complete drug dissolution. The hybrid material was isolated by centrifugation and the cytostatic agent loading was evaluated by UV-VIS spectroscopy by measuring the supernatant solution absorbance at 238 nm. Thermogravimetric analysis was also employed to confirm the drug uptake values. The AGT loaded hybrid materials are denoted “AGT@support;solvent”. For example, the hybrid material obtained using MCM-41 and AGT alcoholic solution is labelled AGT@MCM;EtOH, while drug loaded onto MCM-TG from HCl 1 M aqueous solution has yielded the hybrid material AGT@MCM-TG;HCl 1M.

In vitro aminoglutethimide release studies were performed in a 250 mL glass reactor under magnetic stirring (100 rpm), at 37 °C in “sink” conditions, using a quantity of hybrid sample containing 10 mg drug at a constant volume of 90 mL phosphate buffer solution pH=7.4. The AGT concentration in the release medium was monitored by UV-VIS spectroscopy. Aminoglutethimide dissolution was investigated in the same conditions, employing 10 mg therapeutic agent.

Characterization

Fourier transform infrared spectra (FT-IR) were recorded on a Bruker Tensor 27 spectrometer using the KBr pellets technique. Differential scanning calorimetry (DSC) was performed on a Setaram 131 Evo calorimeter in 30 μ L aluminium pans with pierced lids under N₂ flow at a 10 °C/min. scanning rate. UV-Vis spectra were recorded using an Ocean Optics USB 4000 spectrometer, in 1 cm quartz cuvettes. Thermogravimetric analyses were recorded on a Mettler Toledo GA/SDTA851e equipment, in the temperature range of 30-850 °C, in air using alumina crucibles and a heating rate of 10 °C/min. The SiO₂:3-aminopropyl molar ratio was computed from the organic groups mass loss of MCM-APTES subtracting the weight loss associated to water desorption. For the SiO₂: N-propyl-2-sulfacetamide molar ratio, the water desorption and 3-aminopropyl mass loss was subtracted from the total mass loss. Small- and wide-angle XRD was carried out using a Rigaku MiniFlex II diffractometer with CuK α radiation. Nitrogen adsorption–desorption isotherms were obtained on a Quantachrome Autosorb iQ porosimeter at 77 K. Specific surface area values were determined by the Brunauer–Emmett–Teller (BET) model in the 0.1-0.3 relative pressure range of the isotherm adsorption branch, while pore size distribution was computed using the Barrett-Joyner-Halenda (BJH) theory from the desorption branch. Scanning electron microscopy (SEM) investigation was performed on a Tescan Vega 3 LM electron microscope endowed with an energy-dispersive X-ray spectroscopy (EDX) module.

Logit hydrogen bonding propensity model

The logit hydrogen bonding propensity (LHP) model is a knowledge-based model, which can assess the probability of hydrogen bonding (or “propensity”) between suitable donor and acceptor heteroatoms in a given molecule or group of molecules, based on the existing crystallographic information in the Cambridge Structural Database (CSD v5.34, updated up to February 2013) repository^{25,26}. The Mercury v3.1 software was used to construct the LHP model. The target molecule is described in terms of functional groups containing hydrogen bond donors or acceptors and from all the CSD structures containing at least one functional group, a subset containing the closest matches is then selected. From this “training set” the information pertaining to the environment of the selected functional

groups (such as aromaticity, steric density, competition etc.), as well as the presence or absence of a hydrogen bonding is extracted. A logistic regression of the extracted information is used to build a statistical model, which can predict the probability of hydrogen bonding between each donor-acceptor pair. This propensity takes values between 0 (no hydrogen bonding) and 1 (hydrogen bonding always occurs). The discrimination strength of the model is given by the “area under receiver operating characteristic curve” (AUC) parameter, which denotes the correct identification of hydrogen bonding in the training set using the statistical model, with values between 0 (statistical chance identification) and 1 (correct outcome obtained for all hydrogen bonding in the training set).

For aminoglutethimide, a cyclic imide (-CO-NH-CO-) and aromatic primary amine ($C_{\text{aromatic}}\text{-NH}_2$) groups were considered in the LHP model. In the case of aminoglutethimide hydrochloride charged amine group (-NH_3^+) and chloride (Cl^-) ions were employed instead of the aromatic primary amine moiety. The mesoporous silica surface was approximated by: hydroxyl group bonded to tetravalent silicon (Si-OH), Si-O-Si fragment, aliphatic amine group for MCM-APTES ($C_{\text{aliphatic}}\text{-NH}_2$), aliphatic amide ($C_{\text{aliphatic}}\text{-CO-NH-}C_{\text{aliphatic}}$) and aliphatic thiol groups ($C_{\text{aliphatic}}\text{-SH}$) for MCM-TG. Water (H_2O) was also included. The siloxide anion (Si-O^-) was not employed due to the low occurrence of this group in the CSD.

The training set for uncharged AGT contains 1556 structures (Table S1), with an AUC value of 0.792, while for the aminoglutethimide hydrochloride it is composed of 1437 total structures (Table S2), with an AUC value of 0.799. In both cases, 114 Si-O-Si and 211 Si-OH instances were found in the CSD.

Results and discussion

Carriers characterization

The successful functionalization with aminopropyl groups in the case of MCM-APTES and additional condensation of thioglycolic acid for the MCM-TG matrix were evidenced by FT-IR spectroscopy (Fig. 1). Both functionalized materials present the characteristic silica vibrations at 1080 and 800 cm^{-1} associated with asymmetric and symmetric Si-O-Si stretching vibrations, Si-OH stretching vibrations at 960 cm^{-1} and Si-O-Si bending at 460 cm^{-1} . The bands in the range of 2800–3000 cm^{-1} can be attributed to the stretching C-H vibrations (2978, 2934, 2887 cm^{-1} for MCM-APTES – Fig. 1 A and 2927, 2855 cm^{-1} for MCM-TG - Fig. 1 B). The bending vibrations of amine group (1560 cm^{-1} for MCM-APTES – Fig. 1 A) and the amide characteristic vibrations (1678, 1645 cm^{-1} for MCM-TG – Fig. 1 B) were identified. The lack of carboxylic acid characteristic vibrations at 1720 cm^{-1} in the FTIR spectrum of MCM-TG (Fig. 1 inset) indicates that the thioglycolic group is chemically bound to the silica pore walls through amide bonds.

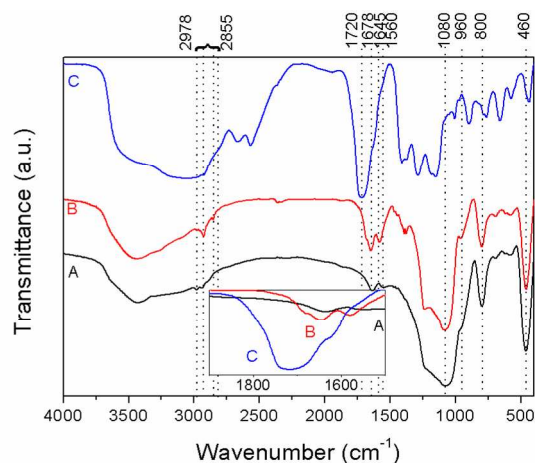


Fig. 1. FT-IR spectra of A) MCM-APTES, B) MCM-TG and C) thioglycolic acid. Inset shows the 1900 - 1500 cm^{-1} region of the spectra for the same compounds

The amount of grafted 3-aminopropyl and N-propyl-2-sulfacetamide groups was quantified by thermogravimetric analysis (Fig. 2). For both functionalized carriers, water molecules desorption caused the mass loss in the 50-130 $^{\circ}\text{C}$ temperature range. The combustion of organic groups bound on silica pore surface of MCM-APTES (9.8% mass loss) and MCM-TG (16.9%) took place ranging from 150 $^{\circ}\text{C}$ to 800 $^{\circ}\text{C}$ in two and three steps, indicating a molar ratio SiO_2 : 3-aminopropyl of 1 : 0.112 and SiO_2 : N-propyl-2-sulfacetamide of 1 : 0.102, respectively. Therefore, MCM-TG contains some unreacted APTES groups, the thioglycolic acid condensation yield being 91 %.

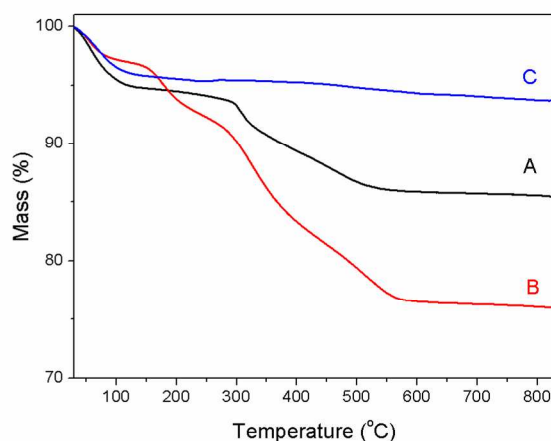


Fig. 2. Thermogravimetric analysis of MCM-APTES (A), MCM-TG (B) and MCM-41 (C)

The small-angle XRD patterns of the mesoporous carriers show three Bragg reflections, (100), (110), (200) belonging to the hexagonal $P6m$ symmetry (Fig. 3). The hexagonal pore array is preserved in

the functionalized MCM-41 materials, although a progressive reduction of the relative intensities for the (110) and (200) Bragg reflections with increasing organic group length can be noticed. This could be explained by the increase in electronic density inside the mesopores caused by the grafting of organic groups.²⁸

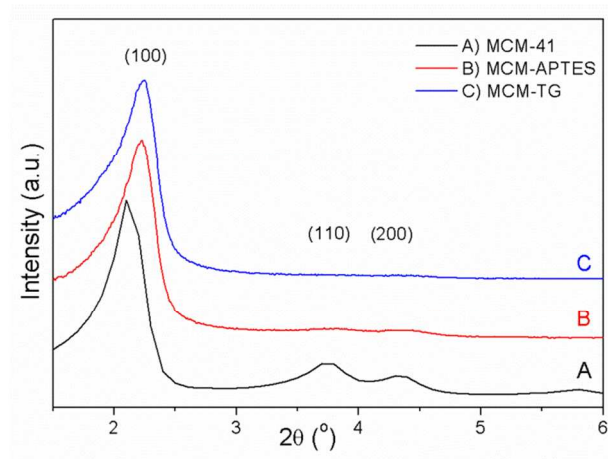


Fig. 3. Small-angle XRD patterns of MCM-41 (A), MCM-APTES (B) and MCM-TG (C)

The three supports present type IV N_2 adsorption-desorption isotherms characteristic for mesoporous materials (Fig. 4). Both functionalized MCM-41 supports show a comparable and marked decrease in the N_2 adsorbed volume as compared with the pristine MCM-41, signifying a partial filling of the mesopores with organic groups bound on the silica pore surface. As expected, increasing the length of the organic substituent leads to a decrease in the average pore size value from 2.97 nm for MCM-41 to 2.13 and 1.87 nm for MCM-APTES and MCM-TG, respectively (Fig. 4 inset). The closing of the hysteresis loop at 0.42 relative pressure is caused by the capillary condensation of nitrogen into the mesoporous channels, resulting in a false peak in the pore size distribution centred at ~ 4 nm.²⁹ The $0.55 \text{ cm}^3 \text{ g}^{-1}$ pore volume value for the MCM-APTES sample is higher than the $0.41 \text{ cm}^3 \text{ g}^{-1}$ pore volume of MCM-TG support (Table 2).

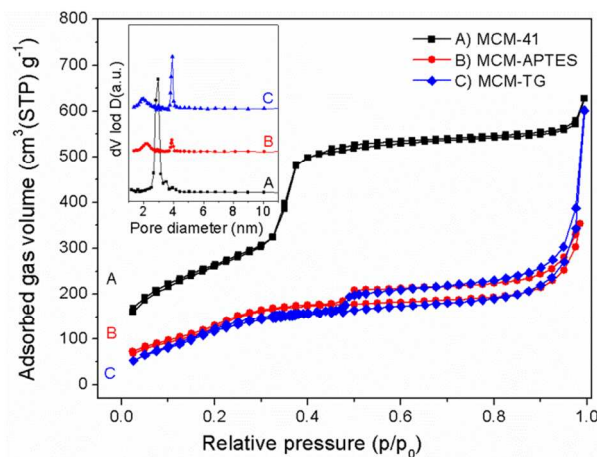


Fig. 4. N_2 adsorption-desorption isotherms for MCM-41 (A), MCM-APTES (B) and MCM-TG (C). Inset shows the pore size distribution for the same materials

Aminoglutethimide loading experiments and characterization of hybrid samples

In order to increase the cytostatic agent uptake, all the drug loading experiments were performed in concentrated solutions, close to the solubility limit of the compound. AGT loading from acetonitrile ($c=100 \text{ gL}^{-1}$) or ethanol ($c=16.7 \text{ gL}^{-1}$) solutions led to a crystalline drug phase on the support surface (Fig. 5), besides the amount adsorbed into the pores. AGT loading from acidic aqueous solutions resulted in hybrid samples with no crystalline drug phase, signifying therapeutic agent adsorption only at the mesopore level. In all cases, a direct relationship between the drug concentration in the initial solution and loading yield has been noticed. For example, experiments using the MCM-41 support and an acidic HCl 0.1 M solution containing 10 gL^{-1} AGT afforded a drug uptake of 12.3 %, while employing a 1 M HCl solution containing 100 gL^{-1} AGT yielded a drug loading of 38.3% (Table 1). Therefore, 1M HCl aqueous solution containing 100 gL^{-1} AGT constitutes the best loading conditions, resulting in high amount of biologically-active compound adsorbed into the mesopores.

Although slightly lower than for MCM-41-based hybrids, good AGT uptake values for the functionalized supports were obtained. However, loading onto the MCM-APTES carrier led to the partial crystallization of AGT, indicated by small intensity diffraction peaks in the wide-angle XRD pattern of AGT@MCM-APTES;HCl 1M (Fig. 5 F).

Table 1. Drug loading conditions, its content in hybrid samples and crystalline drug phase identified by XRD

Hybrid sample	$m_{\text{AGT}}/m_{\text{support}}$ /%wt	Solvent	$C_{\text{AGT}}/\text{g L}^{-1}$	AGT content /%wt.	Crystalline drug phase
AGT@MCM;MeCN	100	MeCN	100	28.8	yes
AGT @MCM;EtOH	100	EtOH	16.7	22.1	yes
AGT @MCM;HCl 0.1M	100	HCl 0.1M	10	12.3	no
AGT @MCM;HCl 1M	100	HCl 1M	100	33.1	no
AGT @MCM;HCl 0.5M	50	HCl 0.5 M	50	20.1	no
AGT @MCM-APTES;HCl 1M	100	HCl 1M	100	27.1	yes
AGT@MCM-TG;HCl 1M	100	HCl 1M	100	22.5	no

The AGT uptake values determined from UV-VIS spectroscopy (Table 1) were in good agreement with the thermogravimetric analysis (data not shown).

The mesopore hexagonal pore array was preserved after AGT loading procedure in all cases, revealed by the presence of the three characteristic Bragg reflections in low angle-XRD patterns (Fig. 5 inset). The wide angle-XRD data of AGT@MCM;MeCN (Fig. 5 A), AGT@MCM;EtOH (Fig. 5 B) and AGT@MCM-APTES;HCl 1M (Fig. 5 F) show the characteristic peaks of crystalline AGT, besides the broad diffraction peak specific for amorphous silica.

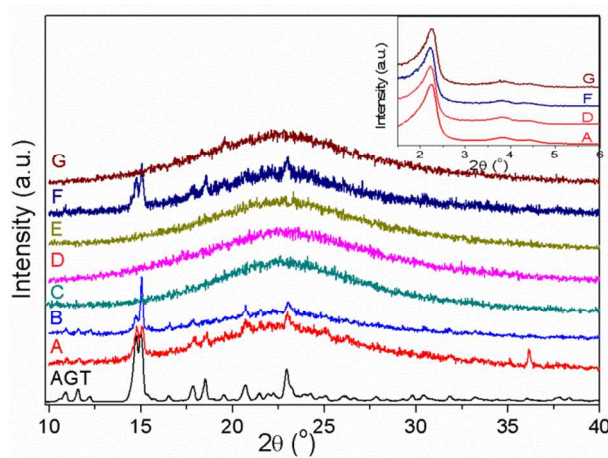


Fig. 5. Wide angle-XRD data of AGT and hybrid samples AGT@MCM;MeCN (A), AGT@MCM;EtOH (B), AGT@MCM;HCl 0.1M (C), AGT@MCM;HCl 1M (D), AGT@MCM;HCl 0.5M (E), AGT@MCM-APTES;HCl 1M (F) and AGT@MCM-TG;HCl 1M (G). Inset shows low angle-XRD patterns of AGT@MCM;MeCN (A), AGT@MCM;HCl 1M (D), AGT@MCM-APTES;HCl 1M (F) and AGT@MCM-TG;HCl 1M (G)

For all hybrid samples, the presence of the drug molecules was evidenced by FT-IR spectroscopy (Fig. 6). The drug crystalline phase formation could be correlated with N-H stretching vibrations (3473 , 3379 cm^{-1} Fig. 6 B, C and E), which are absent for the hybrids containing only amorphous AGT (Fig. 6 D

and F). This fact might be explained by the existence of the drug molecules as charged amines or by the involvement of the amine groups into hydrogen bonding with the surface moieties of the carriers.

Additional information regarding the state of drug phase present in hybrid samples could be ascertained by DSC. The AGT drug shows a sharp endothermic event with $T_{\text{onset}} = 150.9\text{ }^{\circ}\text{C}$, associated with the melting of the bulk crystalline drug. Both the mesoporous supports and hybrid samples present an endothermic event in the 50-125 $^{\circ}\text{C}$ temperature range, assigned to physisorbed water desorption.

All hybrids which show the crystalline AGT peaks in wide-angle XRD data (AGT@MCM;MeCN and AGT@MCM;EtOH – Fig. 5 A and B) also present the endothermic drug melting in DSC traces at the same temperature as bulk AGT ($\sim 151^{\circ}\text{C}$), with the exception of AGT@MCM-APTES; HCl 1M. All other hybrid materials prepared from acidic aqueous solution lack a drug melting event, confirming the amorphous AGT state indicated by wide-angle XRD analyses.

For the AGT@MCM-APTES; HCl 1M material (Fig. 7 F) the drug melting point is lowered with 7 $^{\circ}\text{C}$ ($T_{\text{onset}}=144.2\text{ }^{\circ}\text{C}$). This melting point depression could be explained either by the existence of a different crystalline drug phase in this material (such as a salt, solvate, hydrate or polymorph) or by particle size reduction (nanoscale effect). The decrease of particle size of crystalline substances to the nanometer scale leads to a decrease of their melting and recrystallization points^{30,31}. The wide-angle XRD pattern of AGT@MCM-APTES; HCl 1M contains the most intense characteristic AGT peaks (Fig. 5), suggesting that in this case the melting point depression is caused by the nanoscale effect.

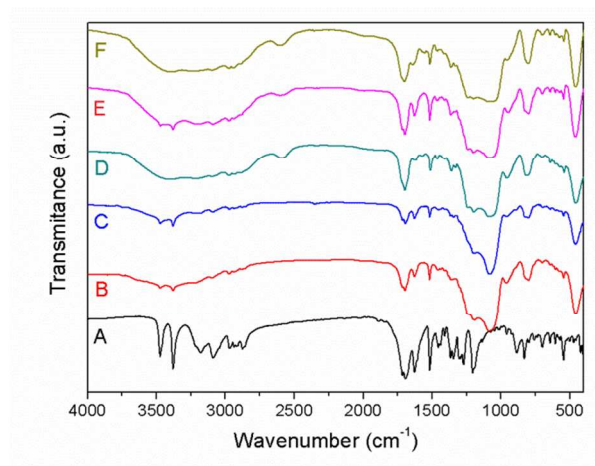


Fig. 6. FTIR spectra of AGT (A), AGT@MCM;MeCN (B), AGT@MCM;EtOH (C), AGT@MCM;HCl 1M (D), AGT@MCM-APTES;HCl 1M (E) and AGT@MCM-TG;HCl 1M (F)

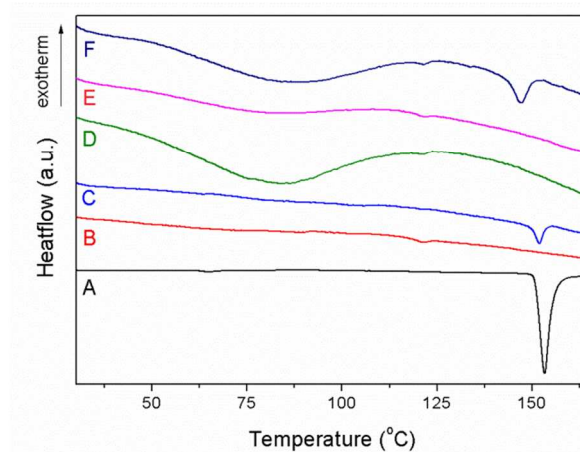


Fig. 7. DSC curves of AGT (A), MCM-41 (B), AGT@MCM;MeCN (C), AGT@MCM;HCl 1M (D), AGT@MCM-TG;HCl 1M (E) and AGT@MCM-APTES;HCl 1M (F)

Nitrogen adsorption-desorption isotherms of hybrid samples containing pristine MCM-41 support, AGT@MCM;HCl 1M and AGT@MCM;HCl 0.5M present lower porosity and the characteristic hysteresis loop of MCM-41-type materials (Fig. 8 A and B). The adsorbed N₂ volume reduction can be explained by the presence of the drug inside the mesochannels, as AGT@MCM;HCl 1M has a higher content of drug and lower porosity. For the hybrid materials the average pore diameter is only slightly reduced in comparison with the MCM-41 support (Table 2), denoting weak interactions between the adsorbate molecules and the support.

In the cases of AGT@MCM-APTES;HCl 1M and AGT@MCM-TG;HCl 1M samples, type II isotherms were recorded (Fig. 8 C and D) characteristic for nonporous materials. As the functionalized supports have lower mesopore volume than MCM-41, the AGT molecules almost completely filled out the mesopores. The lack of porosity of AGT@MCM-APTES;HCl 1M hybrid correlates with the DSC and wide-angle XRD data, as a crystalline AGT can block the accesses of gas molecules to the mesopores (Table 2).

Table 2. Structural and textural parameters of mesoporous supports and hybrids

Samples	a_0 /nm	d_{100} /nm	$d_{B,H}$ /nm	wt /nm	$S_{BET}/m^2 g^{-1}$	$V_{meso}^a/cm^3 g^{-1}$
MCM-41	4.86	4.21	2.97	1.89	959	0.94
MCM-APTES	4.58	3.97	2.13	2.45	620	0.55
MCM-TG	4.54	3.93	1.87	2.67	521	0.41
AGT@MCM;HCl 1M	4.57	3.96	2.72	1.85	95	0.10
AGT@MCM;HCl 0.5M	4.62	4.00	2.67	1.95	435	0.44
AGT@MCM-APTES;HCl 1M	4.58	3.97	1.35	3.23	15	0.01
AGT@MCM-TG;HCl 1M	4.52	3.92	1.87	2.65	36	0.04

^aPore volume computed for pores with diameter lower than 10 nm; *wt* is wall thickness.

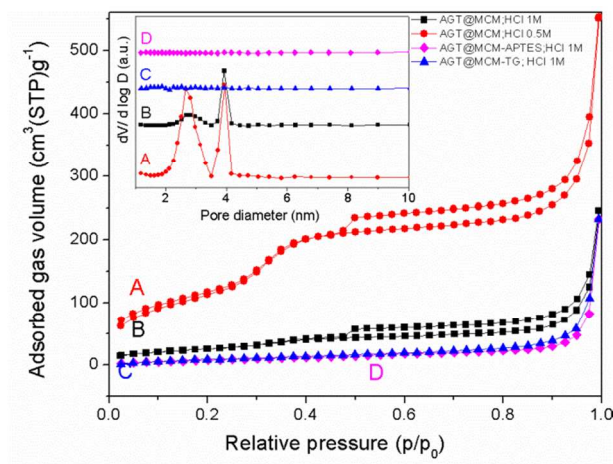


Fig. 8. N₂ adsorption-desorption isotherms for AGT@MCM;HCl 0.5M (A), AGT@MCM;HCl 1M (B), AGT@MCM-TG; HCl 1M (C) and AGT@MCM-APTES;HCl 1M (D). Inset shows the pore size distribution of the same samples

The morphology of supports and hybrids (Fig. 9) consists of spherical particles, forming agglomerates with sizes varying from 100 nm up to 1-2 μm , characteristic for MCM-41-type materials. Drug loading procedure did not alter the morphology of the carriers (Fig. 9 A versus B). The EDX analysis on AGT@MCM-TG;HCl 1M revealed the presence of chlorine atoms.

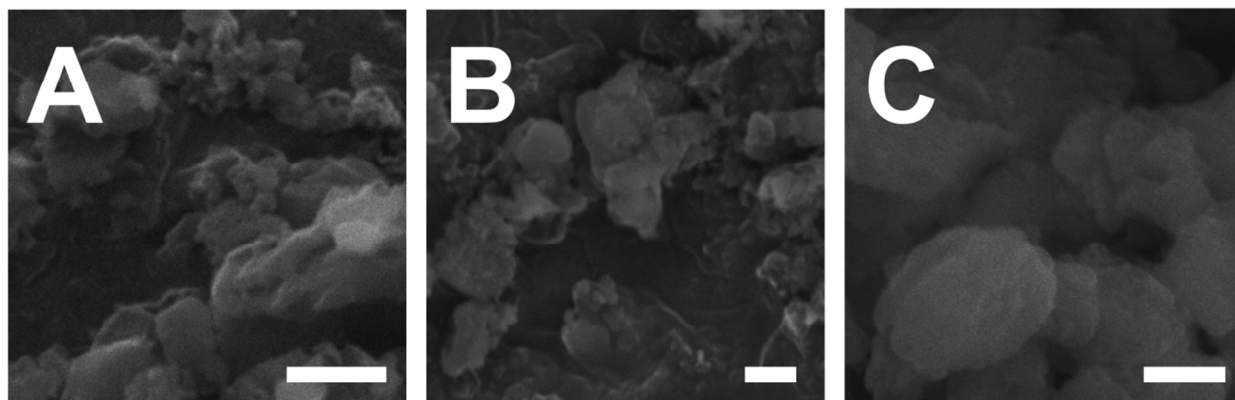


Fig. 9. SEM micrographs of MCM-TG (A), AGT@MCM-TG; HCl 1M (B) and AGT@MCM-APTES; HCl 1M (C). All scale bars are 500 nm.

Aminoglutethimide *in vitro* release

The AGT release profiles in phosphate buffer solution, pH 7.4 at 37 °C were obtained for the hybrid samples. Compared with the bulk crystalline drug dissolution, all hybrid materials exhibited a spectacular increase in drug dissolution rate (Fig. 10). At least 95% of the total drug cumulative release was reached after 15 minutes, while a similar dissolution level for the bulk drug was attained only after 6 h. Particularly for poorly soluble drugs, dissolution rate enhancement can occur after loading onto mesoporous materials³²⁻³⁴. This effect could be explained by the synergetic action of several factors, mainly the large surface area available to the solvent molecules in the case of drugs adsorbed only on the mesopore surface and the existence of biologically-active compound in amorphous state^{35,36}. Considering the large variation in porosity for hybrids (Table 2) and the fast release of all samples, the presence of AGT in mesopores in an amorphous state likely has the main contribution.

High total cumulative release values between 88-100% were obtained for all hybrid samples, with complete release for AGT@MCM-TG1 M HCl and lowest for AGT@MCM-APTES;1 M HCl (Fig. 10).

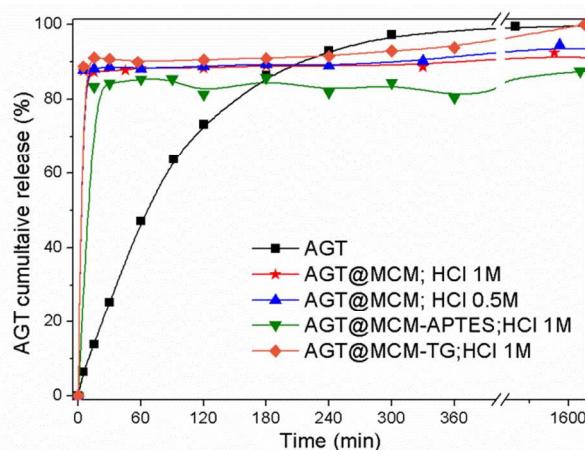


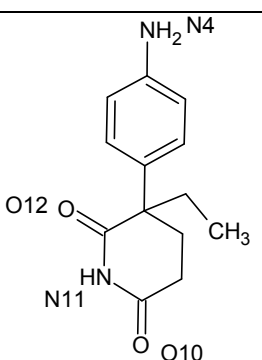
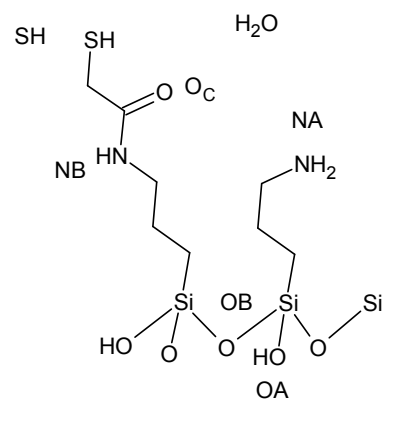
Fig. 10. Aminoglutethimide dissolution and release profiles for hybrid samples

Logit hydrogen bonding propensity model

The LHP propensity model was employed in order to give additional insight into the differences of AGT loading as a neutral or protonated molecule. It was rationalized that the main difference between the two cases will arise from the hydrogen bonding and electrostatic interactions between the AGT molecules and carrier surface groups and not from marked differences in van der Waals forces.

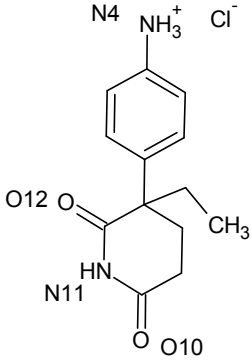
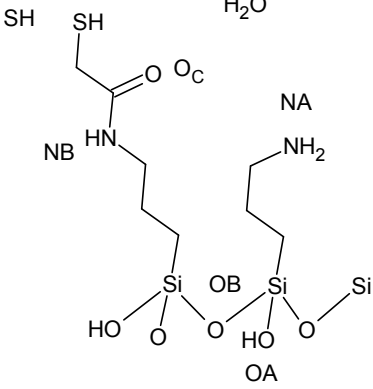
The highest propensity donor-acceptor pairs for uncharged silica fragment, water and uncharged AGT are presented in Table 3, while the corresponding results for the AGT hydrochloride are presented in Table 4. The donor and acceptor atoms are denoted according to the formulas presented in each table.

Table 3. LHP results for neutral AGT, support and water. Only pairs with propensity values greater than 0.70 are presented

Fragment formula	Donor	Acceptor	Propensity	Propensity bounds	Interaction type
	OA	O10	0.98	0.96 - 0.99	Drug - support
	N4	O10	0.97	0.94 - 0.99	Drug - drug
	H ₂ O	O10	0.96	0.92 - 0.98	Drug - water
	NA	O10	0.96	0.92 - 0.98	Drug - support
	NB	O10	0.92	0.85 - 0.96	Drug - support
	OA	OA	0.90	0.85 - 0.93	Support - support
	OA	O12	0.89	0.80 - 0.94	Drug - support
	SH	O10	0.88	0.74 - 0.95	Drug - support
	N11	O10	0.87	0.76 - 0.94	Drug - drug
	N4	OA	0.86	0.78 - 0.91	Drug - support
	H ₂ O	NA	0.85	0.77 - 0.90	Support - support
	OA	OC	0.85	0.77 - 0.90	Support - support
	H ₂ O	OA	0.81	0.72 - 0.88	Support - water
	NA	OA	0.81	0.71 - 0.88	Support - support
	H ₂ O	O12	0.80	0.67 - 0.89	Drug - water
	NA	O12	0.80	0.66 - 0.89	Drug - support
	N4	OC	0.79	0.71 - 0.85	Drug - support
	OA	NA	0.76	0.66 - 0.84	Support - support
	OA	H ₂ O	0.75	0.64 - 0.83	Support - water
	H ₂ O	OC	0.73	0.64 - 0.80	Support - water
NA	OC	0.73	0.63 - 0.81	Drug - support	

For both charged and neutral drugs, it can be seen that the hydrogen bonding interactions between AGT molecules and silanol groups have higher propensities than the drug-drug or support-support interactions. The propensity for hydrogen bonding between N4 or N11 nitrogen atoms and the imide oxygen of AGT is slightly higher for the N4 amine atom (0.97 *versus* 0.87 for N11) and comparable with silanol (0.98). These results indicate that hydrogen bonding is possible between the drug molecule and the pristine and functionalized supports, occurring mostly by silanol – imide oxygen bonds. Generally, the highest propensity bonds are formed between silanol or any nitrogen donors (from AGT and APTES or TG groups) and the O10 acceptor atom of AGT. Hydrogen bonding to the imide O12 atom has lower propensity (Table 3), probably because of steric hindrance of this atom.

Table 4. LHP results for AGT, support and water. Only pairs with propensity values greater than 0.70 are presented

Fragment formula	Donor	Acceptor	Propensity	Propensity bounds	Interaction type
	OA	Cl ⁻	0.98	0.97 - 0.99	Drug - support
	OA	O10	0.98	0.96 - 0.99	Drug - support
	N4	Cl ⁻	0.98	0.97 - 0.99	Drug - drug
	N4	O10	0.98	0.95 - 0.99	Drug - drug
	NA	Cl ⁻	0.97	0.95 - 0.98	Drug - support
	NA	O10	0.97	0.93 - 0.99	Drug - support
	H ₂ O	Cl ⁻	0.96	0.94 - 0.97	Drug - water
	H ₂ O	O10	0.96	0.9 - 0.98	Drug - water
	NB	Cl ⁻	0.93	0.9 - 0.96	Drug - support
	NB	O10	0.92	0.84 - 0.96	Drug - support
	SH	Cl ⁻	0.92	0.86 - 0.95	Drug - support
	N11	Cl ⁻	0.91	0.85 - 0.95	Drug - drug
	SH	O10	0.91	0.79 - 0.96	Drug - support
	OA	OA	0.91	0.86 - 0.94	Drug - drug
	N11	O10	0.90	0.81 - 0.95	Drug - drug
	OA	O12	0.90	0.81 - 0.95	Drug - support
	N4	OA	0.87	0.8 - 0.92	Drug - support
	N4	O12	0.87	0.78 - 0.93	Drug - drug
	NA	OA	0.84	0.76 - 0.9	Support - support
	NA	O12	0.84	0.73 - 0.91	Drug - support
	OA	OC	0.82	0.74 - 0.88	Support - support
	H ₂ O	OA	0.79	0.69 - 0.86	Support - water
	OA	NA	0.79	0.69 - 0.86	Support - support
	H ₂ O	O12	0.78	0.65 - 0.87	Drug - water
	N4	OC	0.78	0.7 - 0.85	Drug - support
	OA	H ₂ O	0.77	0.67 - 0.85	Support - water
	NA	OC	0.73	0.63 - 0.81	Support - support
N4	H ₂ O	0.71	0.62 - 0.78	Drug - water	

In the case of protonated AGT (Table 4), very high propensity (> 0.90) hydrogen bonding is obtained between the N4, N11 AGT donors or all available donor atoms pertaining to the mesoporous supports and the chloride anion. The three highest overall propensity interactions are the silanol - chloride, N4(AGT) – chloride and silanol – imide oxygen hydrogen bonding pairs (all three being 0.98). The support-chloride interactions follow the same trend as the most probable drug-support hydrogen bonding previously discussed, albeit with an increased propensity. These high propensity bonds suggest that supramolecular interactions are easily formed between all the investigated mesoporous supports and

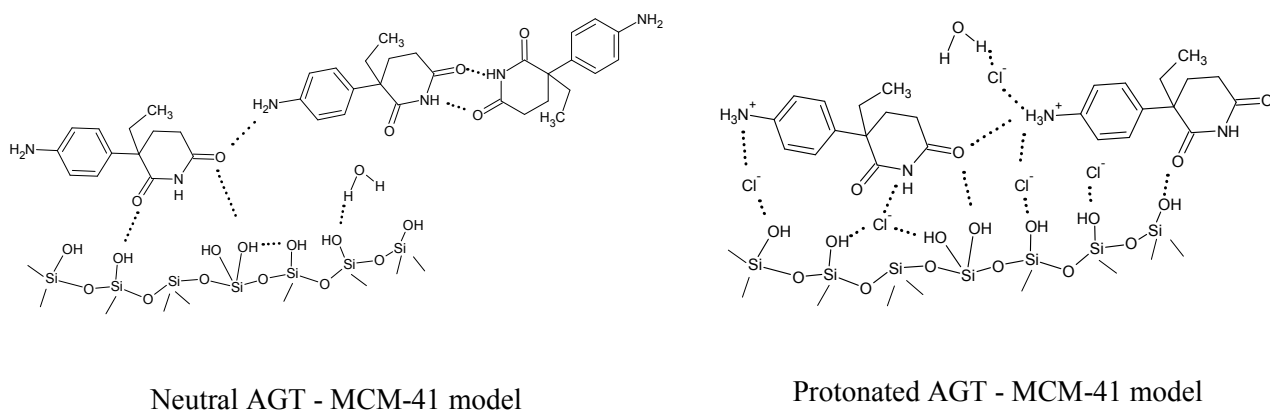
chloride anions present in solution, leading to the anion adsorption onto the support channels surface. In highly acidic conditions, some APTES groups of support are protonated, likely leading to additional strong electrostatic interactions with the chloride anions.

The probability of hydrogen bonding of the support donors can be ranked in decreasing order: silanol > alkyl amine > dialkyl amide > alkyl thiol. The ranking is valid for all hydrogen bonding between mesoporous surface groups and neutral or protonated AGT molecules, as well as for chloride anions.

Regarding the drug-drug hydrogen bonding for the neutral molecule, the LHP model predicts that the strongest interactions occurs between the aromatic amine donor atom N4 and the O12 atom of the imide group. The next probable supramolecular interaction occurs between the N11 and O10 atoms of the imide group. These two interactions are the hydrogen bonds experimentally found in the crystal structure of aminoglutethimide³⁷, supporting the validity of the LHP propensity model.

Based on the model and experimental results we propose that the neutral AGT molecules can form hydrogen bonding with the silanol groups and nitrogen atoms present on the support pore surface. In acidic media, the protonated AGT molecules can form additional attractive electrostatic interactions and hydrogen bonding with the chloride anions bound to the support surface through supramolecular interactions, leading to a stronger adsorption into the pores of supports. At pH=7.4, a fraction of silanol surface groups became deprotonated concomitantly with the neutralization of charged aminoglutethimide molecules. This likely result in repulsive interactions with the chloride anions and diminishes the number of available hydrogen bonding donors for the drug molecules, thus contributing to the rapid release of AGT. A schematic representation of the different AGT interactions as a neutral or ionized molecule with the pore wall of MCM-41 is presented in Scheme 2.

Based on LHP data, one can explain why the total drug cumulative release is highest for the AGT@MCM-TG;1M HCl hybrid material, as the lowest drug-support hydrogen bonding propensities were computed.



Scheme 2. Drug loading on MCM-41 support as neutral and charged aminoglutethimide molecules

Conclusions

For the first time, the incorporation of aminoglutethimide (AGT) into pristine and functionalized mesoporous MCM-41-type silica was investigated. Pristine MCM-41, 3-aminopropyl functionalized MCM-41 and a novel N-propyl-2-sulfanylacetamide-grafted MCM-41 (MCM-TG) were employed for this purpose. The best drug uptake values were obtained when the drug loading was performed in acidic aqueous media, irrespective of the carrier.

Aminoglutethimide *in vitro* release experiments at pH 7.4 show a remarkable increase in drug dissolution rate from the mesoporous silica materials with respect to the bulk crystalline drug. In particular, the novel MCM-TG material represents the best carrier for AGT dissolution rate enhancement, adsorbing 22% wt. drug, which can be reversibly recovered in simulated body fluid, pH 7.4.

A logit hydrogen bonding propensity model was successfully trained and used to quantify the strength of various drug-support supramolecular interactions. These results point out the different AGT adsorption mechanisms in acidic or neutral media and highlight the importance of the chloride anions in AGT adsorption. We propose that positively charged AGT molecules form electrostatic and supramolecular interactions with chloride anions bound to the silica surface through strong silanol-chloride hydrogen bonding ($\text{Si-OH}\cdots\text{Cl}^-\text{AGT}^+$). The lower propensity of hydrogen bonding between drug and the organic groups present on the support pore walls can also explain the high drug cumulative release values from the MCM-TG-based hybrid.

The present study emphasizes the importance of the easily overlooked aspect of drug ionization state and counterions in obtaining hybrid materials. Moreover, one could envision a new possibility to tailor the drug sorption properties of mesoporous silica carriers through careful selection of counterions, affording a modulation of the hydrogen bonding and electrostatic interactions.

The logit hydrogen bonding propensity model proved to be a reliable tool in assessing the supramolecular interactions between the carrier and biologically-active molecules and it could be successfully employed in designing drug delivery systems.

Acknowledgements

The Romanian project PCCA no. 131/2012 is gratefully acknowledged. The work of R.A. Mitran has been supported by the Sectoral Operational Programme Human Resources Development 2007-2013 of the Ministry of European Funds through the Financial Agreement POSDRU/159/1.5/S/132395.

Notes and references

1. C. Argyo, V. Weiss, C. Bräuchle and T. Bein, *Chem. Mater.*, 2013, **26**, 435-451.
2. J. L. Vivero-Escoto, I. I. Slowing, B. G. Trewyn and V. S. Y. Lin, *Small*, 2010, **6**, 1952-1967.
3. W. Xu, J. Riikonen and V.-P. Lehto, *Int. J. Pharm.*, 2013, **453**, 181-197.
4. F. Tang, L. Li and D. Chen, *Adv. Mater.*, 2012, **24**, 1504-1534.
5. L. Bajenaru, D. Berger, L. Miclea, C. Matei, S. Nastase, C. Andronescu, M. G. Moisesescu and T. Savopol, *J. Biomed. Mater. Res. A*, 2014, *in press*, DOI:10.1002/jbm.a.35131.
6. S. Nastase, L. Bajenaru, C. Matei, R. A. Mitran and D. Berger, *Micropor. Mesopor. Mat.*, 2013, **182**, 32-39.
7. S.-Y. Chen, L.-Y. Jang and S. Cheng, *Chem. Mater.*, 2004, **16**, 4174-4180.
8. R.-A. Mitran, D. Berger, L. Băjenaru, S. Nastase, C. Andronescu and C. Matei, *Cent. Eur. J. Chem.*, 2014, **12**, 788-795.
9. J. Kecht, A. Schlossbauer and T. Bein, *Chem. Mater.*, 2008, **20**, 7207-7214.
10. S. K. Natarajan and S. Selvaraj, *RSC Adv.*, 2014, **4**, 14328-14334.
11. M. Kruk, *Accounts Chem. Res.*, 2012, **45**, 1678-1687.
12. J. Fan, C. Yu, F. Gao, J. Lei, B. Tian, L. Wang, Q. Luo, B. Tu, W. Zhou and D. Zhao, *Angew. Chem. Int. Edit.*, 2003, **115**, 3254-3258.
13. M. J. Kim and R. Ryoo, *Chem. Mater.*, 1999, **11**, 487-491.
14. S. Che, Y. Sakamoto, O. Terasaki and T. Tatsumi, *Chem. Mater.*, 2001, **13**, 2237-2239.
15. M. A. Ballem, J. M. Córdoba and M. Odén, *Micropor. Mesopor. Mat.*, 2010, **129**, 106-111.
16. X. Meng, D. Lu and T. Tatsumi, *Micropor. Mesopor. Mat.*, 2007, **105**, 15-23.
17. A. Chang, N.-C. Lai and C.-M. Yang, *RSC Adv.*, 2012, **2**, 12088-12090.
18. E. Samojlik, J. D. Veldhuis, S. A. Wells and R. J. Santen, *J. Clin. Invest.*, 1980, **65**, 602-612.
19. P. E. Lønning and S. Kvinnsland, *Drugs*, 1988, **35**, 685-710.
20. A. Rizk, J. Honegger, M. Milian and T. Psaras, *Clin. Med. Insights Oncol.*, 2012, **6**, 75-84.
21. Z. Guo, X.-M. Liu, L. Ma, J. Li, H. Zhang, Y.-P. Gao and Y. Yuan, *Colloid. Surface. B*, 2013, **101**, 228-235.
22. S.-C. Shen, W. K. Ng, L. Chia, J. Hu and R. B. H. Tan, *Int. J. Pharm.*, 2011, **410**, 188-195.
23. V. Ambrogi, L. Perioli, F. Marmottini, O. Accorsi, C. Pagano, M. Ricci and C. Rossi, *Micropor. Mesopor. Mat.*, 2008, **113**, 445-452.
24. M. Delle Piane, M. Corno and P. Ugliengo, *J. Chem. Theory. Comput.*, 2013, **9**, 2404-2415.
25. P. T. A. Galek, L. Fabian, W. D. S. Motherwell, F. H. Allen and N. Feeder, *Acta Crystall. B-Stru.*, 2007, **63**, 768-782.
26. P. T. A. Galek, L. Fabian and F. H. Allen, *CrystEngComm*, 2010, **12**, 2091-2099.
27. D. Bruhwiler, *Nanoscale*, 2010, **2**, 887-892.
28. M. Impérator-Clerc, P. Davidson and A. Davidson, *J. Am. Chem. Soc.*, 2000, **122**, 11925-11933.
29. A. H. Janssen, A. J. Koster and K. P. de Jong, *J. Phys. Chem. B*, 2002, **106**, 11905-11909.
30. J. Riikonen, J. Salonen and V.-P. Lehto, *J Therm Anal Calorim*, 2011, **105**, 811-821.
31. M. Beiner, Rengarajan, S. Pankaj, D. Enke and M. Steinhart, *Nano Lett.*, 2007, **7**, 1381-1385.
32. V. Ambrogi, L. Perioli, C. Pagano, F. Marmottini, M. Ricci, A. Sagnella and C. Rossi, *Eur. J. Pharm. Sci.*, 2012, **46**, 43-48.
33. Y. Zhang, Z. Zhi, T. Jiang, J. Zhang, Z. Wang and S. Wang, *J. Controll. Release*, 2010, **145**, 257-263.
34. M. Van Speybroeck, R. Mols, R. Mellaerts, T. D. Thi, J. A. Martens, J. V. Humbeeck, P. Annaert, G. V. d. Mooter and P. Augustijns, *Eur. J. Pharm. Biopharm.*, 2010, **75**, 354-365.
35. V. Ambrogi, L. Perioli, F. Marmottini, S. Giovagnoli, M. Esposito and C. Rossi, *Eur. J. Pharm. Sci.*, 2007, **32**, 216-222.
36. M. Van Speybroeck, R. Mellaerts, R. Mols, T. D. Thi, J. A. Martens, J. Van Humbeeck, P. Annaert, G. Van den Mooter and P. Augustijns, *Eur. J. Pharm. Sci.*, 2010, **41**, 623-630.

37. P. Van Roey, K. A. Bullion, Y. Osawa and D. G. Braun, *Acta Crystallogr. C*, 1991, **47**, 829-832.